

Article

Mode Coupling Properties of the Plasmonic Dimers Composed of Graphene Nanodisks

Houbo Chen ¹, Weibin Qiu ^{1,*}, Pingping Qiu ¹, Junbo Ren ¹, Zhili Lin ¹, Jia-Xian Wang ¹, Qiang Kan ² and Jiao-Qing Pan ²

¹ Fujian Key Laboratory of Light Propagation and Transformation, College of Information Science and Engineering, Huaqiao University, No. 668, Jimei Avenue, Jimei District, Xiamen 361021, China; 1400201017@hqu.edu.cn (H.C.); 1511301022@hqu.edu.cn (P.Q.); 1611301026@hqu.edu.cn (J.R.); zllin@hqu.edu.cn (Z.L.); wangjx@hqu.edu.cn (J.-X.W.)

² Institute of Semiconductors, Chinese Academy of Sciences, 35A, Qinghua East Road, Haidian District, Beijing 100086, China; kanqiang@semi.ac.cn (Q.K.); jqpan@semi.ac.cn (J.-Q.P.)

* Correspondence: wbqiu@hqu.edu.cn; Tel.: +86-133-9501-0121

Academic Editor: Philippe Lambin

Received: 16 January 2017; Accepted: 30 March 2017; Published: 5 April 2017

Abstract: The electromagnetic properties of the plasmonic dimer composed of coupled graphene nanodisks are numerically investigated in this paper. The results demonstrate that the degeneracy of the plasmonic modes of the dimer is lifted when the coupling is introduced. The evolution of the plasmonic mode, with the variation of inter-disk distance and the chemical potential of one of the nanodisks, is studied. The proposed structure might find broad areas of application including light–matter interaction, optical switching, directional emission of the plasmonic emitter, etc.

Keywords: graphene; plasmonic dimer; mode coupling

1. Introduction

Similar to electronic atom and molecule systems, photonic molecules (PhMs) and plasmonic molecules (PMs) are composed of interacting nanostructures in which the specific collective electromagnetic (EM) behaviors are demonstrated [1,2]. These behaviors include Fano resonance [3–5], slow light [6,7], EM-induced transparency [8–10] etc., which result from the coupling between the plasmons and the external disturbance. In the past decade, PhMs and PMs have found significant applications in broad areas including fundamental sciences, the processing of information and biochemics due to their excellent properties of high quality (Q) factors, flexible structure design, and high sensitivity to the variation of the environments [11]. Among the reported works, Qiang Li et al. [12] proposed and fabricated a hybrid photonic–plasmonic molecule composed of two coupled identical Ag–Al₂O₃–Si sandwich disks. This hybrid photonic–plasmonic molecule has sub-wavelength properties and provides a novel platform for the exploration of the light–matter interaction. Sang Wook Kim et al. [13] reported the energy-level evolution of coupled non-identical microdisks (CNMs), which were characterized by their avoided crossing which is intrinsically associated with the exceptional point or the non-Hermitian degeneracy. Svetlana V. Boriskina [14] analyzed the wavelength of the Q factors of the whispering-gallery (WG) modes in the PhM micro-disks as a function of the parameter of the PhM numerically, and demonstrated the crossing and avoid-crossing characteristics. However, all the above-mentioned micro or nanodisk based cavities were made by a conventional novel metal such as Ag and Au, or by dielectric materials such as SiO₂. Thus, the huge ohmic loss would degrade the properties of the devices, for example, Q factors. Furthermore, frequency tunability is impossible as long as the geometric structures of the devices are determined. All the intrinsic shortcomings of the conventional plasmonic materials become an obstacle to practical application.

Recently, graphene, which is composed of a single layer of carbon atoms arranged in a two-dimensional (2D) honeycomb lattice, has attracted great attention in the fields of electronics and photonics all over the world due to its excellent material properties [15–17]. More specifically, in the field of the plasmonics, graphene offers the advantages of high confinement capability, low damping loss and tunability of working frequency. Consequently, graphene is a reliable material to substitute conventional metal materials in the field of plasmonics.

Zhu X. et al. investigated plasmon–phonon coupling in large-area graphene dot and antidot arrays [18]. Rosolen G. and Maes B. reported asymmetric and connected graphene dimers for a tunable plasmonic response [19]. Hadad Y. et al. showed that an electrically small chemical potential interruption in a graphene layer may possess a quasi-static resonance that launches a mixed-type semilocalized plasmon wave [20]. They also designed a system that is extremely sensitive to the quantized spectrum of graphene Landau levels and predicted up to 90° of Faraday rotation with just a single sheet of graphene [21]. We have proposed and numerically explored the plasmonic dimers composed of coupled graphene nanodisks of different sizes, which are surrounded by another chemical potential on the same piece of infinite graphene monolayer [22]. The split modes with non-degenerate wavelengths appear in the proposed structure. Further, the coupling between fundamental and first order WG modes has been pointed out. In the current work, we further analyze the field properties of the collective mode including the resonant frequency; the Q factor in a graphene plasmonic dimer with different chemical potentials in each nanodisk; and we discuss the physical principles behind the EM behaviors of the dimers. The proposed plasmonic molecules could find broad areas of application in fields including tunable filters [23], optical sensors [24] and optical switchers [25].

2. Models and Simulation Method

The 2D schematic of the plasmonic dimer molecule composed of graphene nanodisks is illustrated in Figure 1, where R is the radius of the nanodisks; g is the gap between the two nanodisks; the chemical potential of each nanodisk is μ_{c2} and μ_{c3} , respectively. The chemical potential of the infinite area is μ_{c1} . Perfectly matched layer (PML) is employed as the boundary condition in order to avoid the reflected wave at the boundaries. In this article, the plasmonic properties of the dimers are investigated by utilizing the commercially available software COMSOL Multi-physics, RF module, eigen frequency solver. The graphene monolayer is modeled as an ultrathin film which can be characterized by the effective index defined as $n_{\text{eff}} = \beta/k_0$, where $k_0 = 2\pi/\lambda$ is the wavenumber in free space [26]. The propagation constant of surface plasmon polaritons (SPPs) supported by monolayer graphene can be written as [27,28]

$$\beta = k_0 \sqrt{1 - \left(\frac{2}{\eta_0 \sigma_g} \right)^2} \tag{1}$$

where η_0 (377 Ω) is the intrinsic impedance of the air, which can be expressed by $(\mu_0/\epsilon_0)^{1/2}$ where μ_0 and ϵ_0 represent the permeability and permittivity of vacuum, respectively. The surface conductivity of graphene σ_g , composed of the interband electron transitions σ_{inter} and the intraband electron–photon scattering σ_{intra} , is given by the Kubo formula [17,27–29],

$$\sigma_g = \sigma_{\text{intra}} + \sigma_{\text{inter}} \tag{2}$$

with

$$\sigma_{\text{intra}} = \frac{-ie^2 k_B T}{\pi \hbar^2 (\omega - i/\tau)} \left[\frac{\mu_c}{k_B T} + 2 \ln \left(1 + \exp \left(-\frac{\mu_c}{k_B T} \right) \right) \right] \tag{3}$$

$$\sigma_{\text{inter}} = \frac{-ie^2}{2h} \ln \left[\frac{2|\mu_c| - \hbar(\omega - i/\tau)}{2|\mu_c| + \hbar(\omega - i/\tau)} \right] \tag{4}$$

where μ_c is the chemical potential of graphene; ω is the angular frequency of the plasmon; \hbar is the reduced Planck’s constant; e is the electron charge; k_B is the Boltzmann’s constant; T is the temperature;

and τ is the electron momentum relaxation time. Specifically, the chemical potential of graphene is tunable by either chemical doping or external electrical gating locally [27,30]. Pioneering work showed that a chemical potential as high as 2 eV has been obtained experimentally [31]. Also, a relaxation time as high as 3ps has been achieved experimentally [32]. Thus, in this paper, a relaxation time less than 1ps and a chemical potential less than 1 eV are chosen, which are conservative enough to ensure the reliability of our calculation.

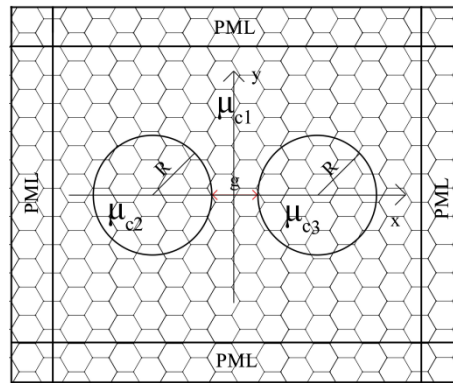


Figure 1. The 2D schematic of the graphene nanodisk dimer molecule, where R is the radius of the nanodisk; μ_{c2} and μ_{c3} are the chemical potentials of each nanodisk.

3. Results and Discussion

When two nanodisks approach each other, the EM fields of the plasmon interact, and the collective modes appear. First, we study the collective resonant EM mode field distribution as a function of the gap between the two nanodisks, where $\mu_{c2} = \mu_{c3} = 0.5$ eV, $\mu_{c1} = 0.1$ eV and $R = 50$ nm. The z component of the typical electric field distribution of $TM_{2,1}$ modes of the dimer with a gap of 0 nm and 15 nm are illustrated in Figure 2a,b, respectively. According to the symmetry with respect to the X and Y directions, the four categories of the graphene plasmonic dimer modes are defined as $[|+1\rangle_x, |+1\rangle_y]$, which is symmetric with respect to both the X and Y directions; $[|+1\rangle_x, |-1\rangle_y]$, which is symmetric with respect to the X direction and anti-symmetric with respect to the Y direction; $[|-1\rangle_x, |+1\rangle_y]$, which is anti-symmetric with respect to the X direction and symmetric with respect to the Y direction; and $[|-1\rangle_x, |-1\rangle_y]$, which is anti-symmetric with respect to both the X and Y direction. More specifically, we follow Ref. [12] and regard the modes which are anti-symmetric with respect to the Y direction as the anti-bonding modes. Normally, the anti-bonding modes are located at the higher energy states. On the other hand, the modes that are symmetric with respect to the Y direction are regarded as the bonding modes, and are located at the lower energy states [12]. The frequency and the quality (Q) factor of the collective modes, as a function of the gap g , are plotted in Figure 3a,b, respectively. It is shown in Figure 3a that the frequencies of the anti-bonding modes decrease with the increasing of the gap g , while the counterparts of the bonding modes demonstrate the converse trend. The coupling strength between the WG modes of the nanodisks is indicated by the frequency splitting of the bonding or anti-bonding modes. When the gap g increases, the coupling strength between the plasmonic modes of the individual nanodisks degrades. Thus, the frequency splitting of the anti-bonding and the bonding modes decreases accordingly [12]. When g further increases to more than 50 nm, all the four mode categories combine together, the result of which is identical to the resonant mode of a single isolated nanodisk. This means that there is no interaction between the two nanodisks of the dimer.

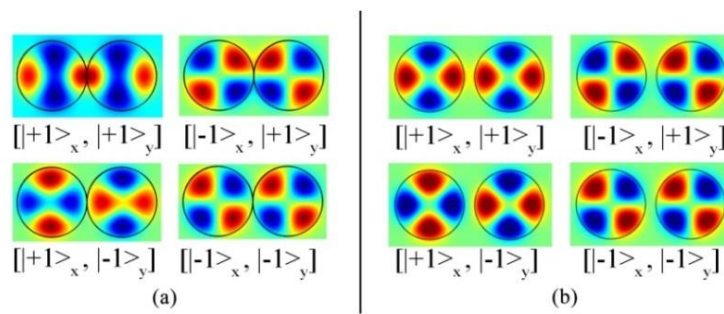


Figure 2. The electric field z component distribution of the collective mode $TM_{2,1}$. (a) $g = 0$ nm and (b) $g = 15$ nm.

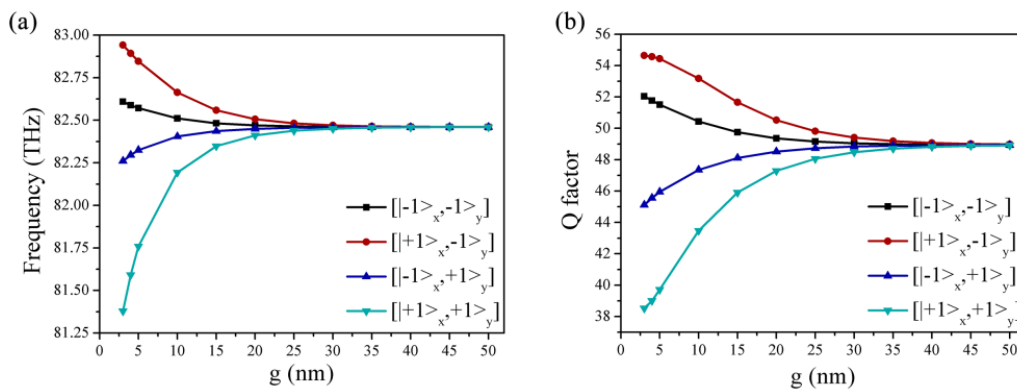


Figure 3. (a) Frequency and (b) Q factor of the collective modes $TM_{2,1}$ as a function of g of the four categories of symmetry, where $\mu_{c2} = \mu_{c3} = 0.5$ eV, $\mu_{c1} = 0.1$ eV and $R = 50$ nm.

It is also shown in Figure 3b that the Q factor of the collective plasmonic mode of the graphene dimer demonstrates an identical trend to that of the resonant frequency as a function of the gap g . To understand this behavior, we plot the real part and imaginary part of the propagation constant β as a function of frequency in Figure 4, where the chemical potential is 0.5 eV. In general, the Q factor is given by $Q_{total}^{-1} = Q_{rad}^{-1} + Q_{abs}^{-1}$ [33,34], where Q_{rad} relates to the radiation loss and Q_{abs} relates to the absorption loss. The radiation loss is determined by the radius and material of the cavity, and Q_{abs} is calculated by

$$Q_{abs} = \frac{\text{Re}(\beta)}{2 \times |\text{Im}(\beta)|} \tag{5}$$

where $\text{Re}(\beta)$ and $|\text{Im}(\beta)|$ are the real part and the absolute value of the imaginary part of the propagation constant β . For a graphene sheet with a chemical potential of 0.5 eV, when the frequency of the plasmon increases from 80 THz to 83.5 THz, $\text{Re}(\beta)$ and $|\text{Im}(\beta)|$ increase together. However, the rising rate of $\text{Re}(\beta)$ is even much faster than $2|\text{Im}(\beta)|$. Consequently, the Q factor increases as the increasing of frequency, and finally results in a similar frequency trend as a function of given g , which are shown in Figure 3a,b.

Next, we investigate the frequency splitting ΔF of the corresponding anti-bonding and bonding modes as a function of the azimuthal mode number m of the plasmonic WG mode $TM_{m,1}$ of the graphene dimers. Figure 5 shows the frequency splitting ΔF of bonding and anti-bonding of WG modes as a function of m , where the distance g is 5 nm. When the azimuthal number increases from 2 to 8, the frequency ΔF of the bonding mode decreases from 0.567 to 0.002 THz, while the counterpart of the anti-bonding mode decreases from 0.275 to 0.0002 THz. When the azimuthal number increases, the wavelength reduces. However, the EM field confinement capacity of the graphene dimer becomes stronger as the resonant wavelength decreases. So the coupling between the plasmonic modes of the

nanodisks becomes weaker, which further results in the small frequency splitting for both the bonding and anti-bonding mode, as shown in Figure 5.

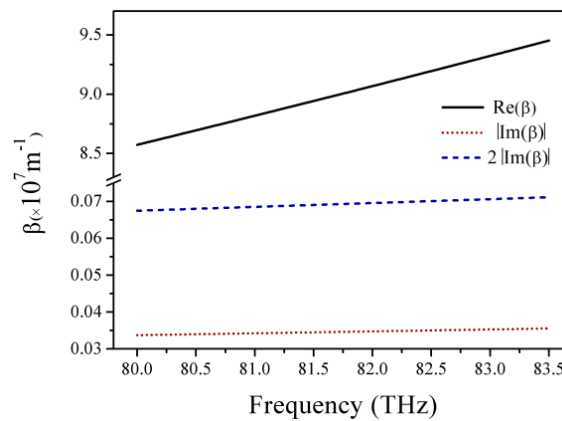


Figure 4. The real part and the absolute value of the imaginary part of the propagation constant as a function of frequency, where the chemical potential of the graphene is 0.5 eV, respectively.

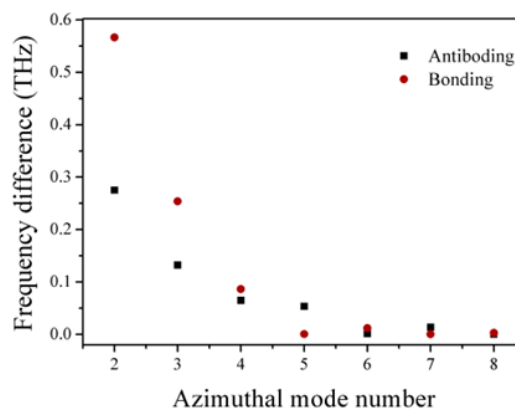


Figure 5. The frequency splitting ΔF of bonding and anti-bonding whispering-gallery (WG) modes of $TM_{m,1}$ as a function of m from 2 to 8, where the distance g is 5 nm.

Then, we study the frequency and the Q factor of the plasmonic mode $TM_{2,1}$ of the graphene plasmonic dimer as a function of the chemical potential of the nanodisk at the right side. Figure 6a,b plots the resonant frequency and the corresponding Q factor as a function of μ_{c3} for the four mode categories. In the range from 0.25 to 0.5 eV, one can see that the frequencies of the two modes which are anti-symmetric with respect to the X direction, i.e., $[|-1\rangle_x, | +1\rangle_y]$ and $[|-1\rangle_x, |-1\rangle_y]$ modes, are similar. There is a notch in the Q factor of the $[|-1\rangle_x, |-1\rangle_y]$ mode at $\mu_{c3} = 0.33$ eV, while there is a peak in the counterpart of the $[|-1\rangle_x, | +1\rangle_y]$ mode at the same point. This is a typical avoid-crossing point [11,14]. However, unlike the photonic dimer composed of the coupled dielectric micro-disks, the Q factors of the $[|-1\rangle_x, | +1\rangle_y]$ and $[|-1\rangle_x, |-1\rangle_y]$ modes demonstrate a general climbing trend as the μ_{c3} increases. This is due to the fact that the mismatching between the plasmons inside and outside the nanodisks becomes stronger when μ_{c3} becomes higher, which also prevents the plasmons from escaping from the nanodisk and eventually results in a general increasing of the Q factor. In order to analyze the avoid-crossing property, we study the EM mode evolution as a function of μ_{c3} and the corresponding diagrams are shown in Figure 7. For the $[|-1\rangle_x, |-1\rangle_y]$ mode, when μ_{c3} reduces from 0.5 to 0.425 eV, the resonant frequency remains stable at a platform of 82.5 THz. Also, the EM field of the left nanodisk does not change significantly and remains in the $TM_{2,1}$ mode. However, the EM field of the right nanodisk is first weakened, then is enhanced again and switched from the $TM_{2,1}$ mode

to the $TM_{3,1}$ mode. When μ_{c3} reduces from 0.425 to 0.34 eV, the EM field in the right disk remains stable in the $TM_{3,1}$ mode. However, the counterpart in the left disk is first weakened then is enhanced again. Also, it switches from the $TM_{2,1}$ mode to the $TM_{1,1}$ mode, and the resonant frequency reduces linearly from 83 to 72 THz with μ_{c3} . When μ_{c3} further decreases from 0.34 to 0.325 eV, another resonant frequency platform appears at 72 THz. The EM mode of the left disk remains in the $TM_{1,1}$ mode, and the field in the right disk is first weakened then enhanced again; the corresponding mode switches from $TM_{3,1}$ to $TM_{1,2}$. When μ_{c3} further reduces to less than 0.325 eV, the plasmonic field in the right disk remains in the $TM_{2,1}$ mode, but the field in the left disk disappears. Meanwhile, the resonant frequency decreases linearly with the reduction of μ_{c3} . As for the $[|-1\rangle_x, | +1\rangle_y]$ mode, when μ_{c3} reduces from 0.5 to 0.4 eV, the plasmonic mode in the right disk remains stable in the $TM_{2,1}$ mode, while the mode in the left disk is first weakened and then enhanced. Also, the plasmonic mode switches from the $TM_{2,1}$ mode to the $TM_{1,1}$ mode in the left disk. At the same time, the resonant frequency decreases linearly from 83 THz to 71 THz with the reduction of μ_{c3} . Similar to the behavior of the $[|-1\rangle_x, | +1\rangle_y]$ mode, a resonant frequency platform appears at around 71 THz when μ_{c3} decreases from 0.4 to 0.33 eV. In this region, the plasmonic mode of the left disk remains stable in the $TM_{1,1}$ mode, and the mode of the right disk is weakened first and then enhanced; also, the $TM_{2,1}$ mode is switched to the $TM_{3,1}$ mode. When μ_{c3} further reduces to less than 0.325 eV, the mode field in the left disk weakens gradually and then eventually disappears. However, the right disk remains in the $TM_{3,1}$ mode. Meanwhile, the resonant frequency decreases with the reduction of μ_{c3} . It should be noted that the bonding/anti-bonding state of the dimmer may be changed during the mode evolution procedure [35].

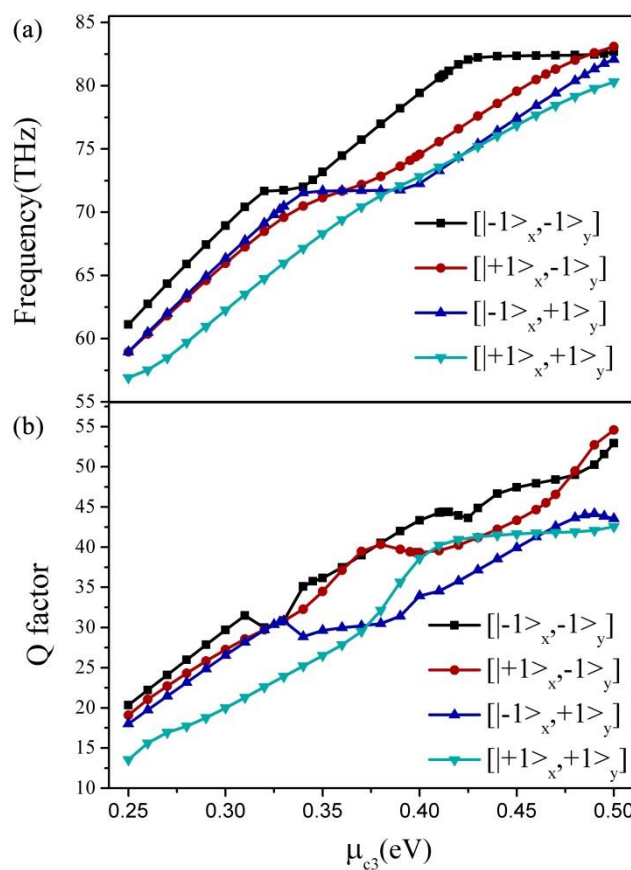


Figure 6. The variation of the frequency and Q factor of the fundamental mode as a function of the chemical potential μ_{c3} . (a) Resonance frequency; (b) Q factor.

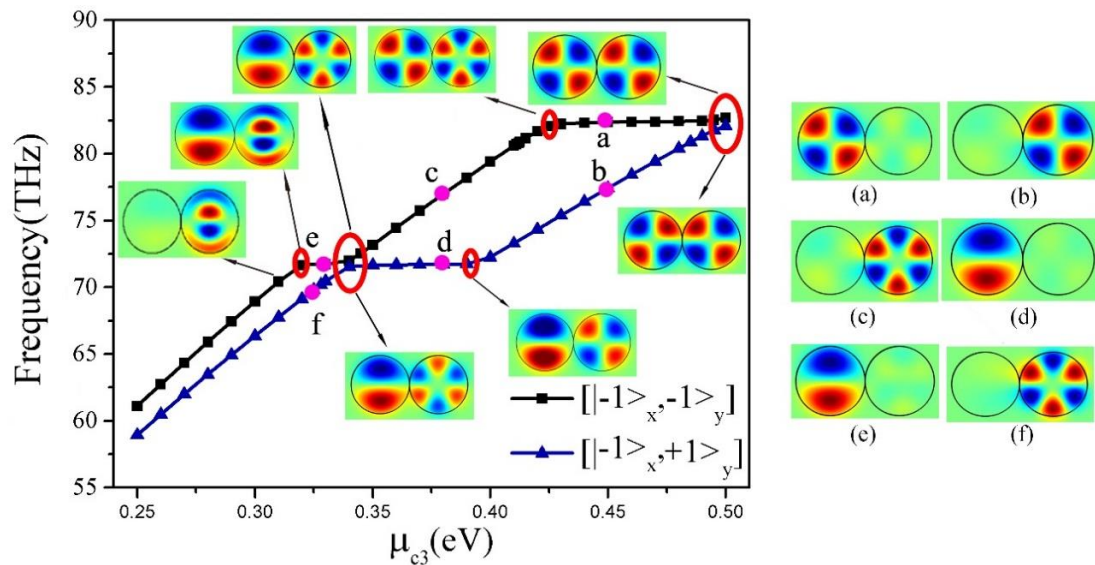


Figure 7. The frequencies of $[|-1\rangle_x, |-1\rangle_y]$ and $[|-1\rangle_x, +1\rangle_y]$ modes as a function of the chemical potential μ_{c3} .

As for the modes which are symmetric with respect to the X axis, $[|+1\rangle_x, +1\rangle_y]$ and $[|+1\rangle_x, -1\rangle_y]$, there is also an avoided-crossing point at around 0.4 eV, which is shown in Figure 6. However, it is not as obvious as that of the asymmetric cases. This may be due to the large frequency splitting, which prevents the strong coupling effect between these two modes.

Figure 8 plots the resonance frequency of the $[|+1\rangle_x, +1\rangle_y]$ mode as a function of μ_{c3} in a range from 0.25 to 0.5 eV with a gap distance from 0 to 15 nm. The insets show the details in a range between 0.37 and 0.42 eV. Interestingly, with the increasing of the gap distance, the “platform” effect on the resonance frequency becomes more significant, accompanied by the red-shift of the peak position of the Q factor. When the chemical potential μ_{c3} decreases and passes the avoided-crossing point, i.e., 0.4 eV, the EM fields of the two nanodisks react with each other and result in the resonant frequency splitting, which is indicated in Figure 8a, accompanied by the appearance of the “platform” effect, peak of the Q factor, and the switching of the EM field distribution. Nevertheless, when the distance gap g reduces, the coupling becomes stronger, and the “platform” effect becomes weaker, which means that it is not necessary to “accumulate” the frequency reduction to ensure the EM field distribution switching. Also, the peak position of the Q factor shows a blue-shift as shown in Figure 8b.

4. Conclusions

In this paper, we proposed and numerically analyzed the EM properties of a plasmonic dimer composed of coupled graphene nanodisks. The resonant frequency and the corresponding Q factor of the anti-bonding mode increase as the distance gap increases between the nanodisks, while the opposite trend is observed in the case of the bonding mode. The frequency difference of both the anti-bonding modes and the bonding modes of the $TM_{m,1}$ reduces as the azimuthal number m increases. An avoided-crossing property has been found in the anti-bonding modes when the chemical potential of the right disk μ_{c3} decreased from 0.5 to 0.25 eV. In the future, more profound graphene nanoclusters will be constructed by adding more nanodisks for the investigation of dynamically tunable Fano resonance lineshape [36] and high order Fano resonance [37], where the graphene nanostructures interact with the external incident EM sources. Another graphene monolayer would be introduced underneath the graphene nanostructures separated by a dielectric spacer [38–40]. The proposed structure might offer a broad range of applications in both scientific and engineering fields such as light–matter interaction, tunable optical filters, and optical sensors.

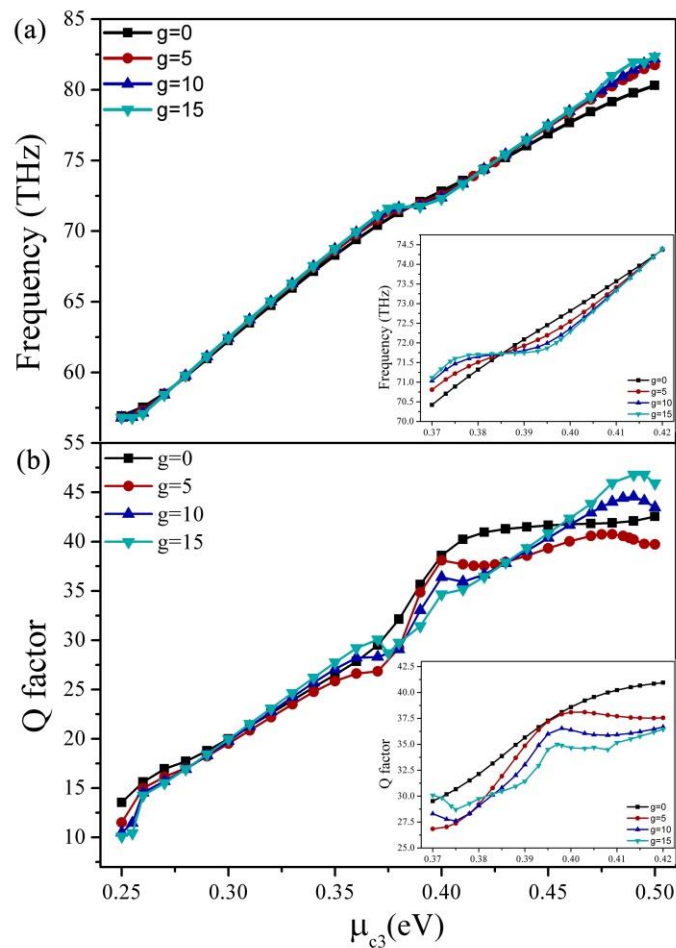


Figure 8. The resonant frequency and the corresponding Q factor as a function of chemical potential μ_{c3} with various gap distances. The insets show the details with a chemical potential from 0.39 to 0.41 eV. (a) Resonance frequency; (b) Q factor.

Acknowledgments: The authors are grateful to the support by the Natural Science Fund of China under grant No. 61378058, the Science and Technology Fund of Quanzhou under grant No. Z1424009, Fujian Province Science Fund for Distinguished Young Scholars (No. 2015J06015) and the Promotion Program for Young and Middle-Aged Teachers in Science and Technology Research of Huaqiao University (No. ZQN-YX203).

Author Contributions: Weibin Qiu provided the original idea; Houbo Chen designed the models; Houbo Chen, Pingping Qiu, and Junbo Ren performed the simulations; Zhili Lin, Houbo Chen, Pingping Qiu, Junbo Ren, Jia-Xian Wang, Qiang Kan and Jiao-Qing Pan analyzed the data; Houbo Chen and Weibin Qiu wrote the paper.

Conflicts of Interest: The authors declare no conflict of interest.

References

1. Chuntonov, L.; Haran, G. Trimeric plasmonic molecules: The role of symmetry. *Nano Lett.* **2011**, *11*, 2440–2445. [[CrossRef](#)] [[PubMed](#)]
2. Chuntonov, L.; Haran, G. Effect of Symmetry Breaking on the Mode Structure of Trimeric Plasmonic Molecules. *J. Phys. Chem. C* **2011**, *115*, 19488–19495. [[CrossRef](#)]
3. Fan, J.A.; Bao, K.; Wu, C.; Bao, J.; Bardhan, R.; Halas, N.J.; Manoharan, V.N.; Shvets, G.; Nordlander, P.; Capasso, F. Fano-like interference in Self-Assembled plasmonic quadrumer clusters. *Nano Lett.* **2010**, *10*, 4680–4685. [[CrossRef](#)] [[PubMed](#)]
4. Hentschel, M.; Saliba, M.; Vogelgesang, R.; Giesse, H.; Alivisatos, A.P.; Liu, N. Transition from Isolated to Collective Modes in Plasmonic Oligomers. *Nano Lett.* **2010**, *10*, 2721–2726. [[CrossRef](#)] [[PubMed](#)]

5. Luk'Yanchuk, B.; Zheludev, N.I.; Maier, S.A.; Hals, N.J.; Nordlander, P.; Giessen, H.; Chong, C.T. The Fano resonance in plasmonic nanostructures and metamaterials. *Nat. Mater.* **2010**, *9*, 707–715. [[CrossRef](#)] [[PubMed](#)]
6. Feng, S.; Gan, L. Multi-channel slow light coupled-resonant waveguides based on photonic crystal with rectangular microcavities. *Opt. Commun.* **2015**, *341*, 257–262. [[CrossRef](#)]
7. Papasimakis, N.; Fedotov, V.A.; Zheludev, N.I.; Prosvirnin, S.L. Metamaterial analog of electromagnetically induced transparency. *Phys. Rev. Lett.* **2008**, *101*, 253903. [[CrossRef](#)] [[PubMed](#)]
8. Liu, N.; Langguth, L.; Weiss, T.; Kastel, J.; Fleischhauer, M.; Pfau, T.; Giessen, H. Plasmonic analogue of electromagnetically induced transparency at the Drude damping limit. *Nat. Mater.* **2009**, *8*, 758–762. [[CrossRef](#)] [[PubMed](#)]
9. Liu, N.; Weiss, T.; Mesch, M.; Langguth, L.; Eigenthaler, U.; Hirscher, M.; Sonnichsen, C.; Giessen, H. Planar metamaterial analogue of electromagnetically induced transparency for plasmonic sensing. *Nano Lett.* **2010**, *10*, 1103–1107. [[CrossRef](#)] [[PubMed](#)]
10. Mukherjee, S.; Sobhani, H.; Lassiter, J.B.; Bardhan, R.; Nordlander, P.; Halas, N.J. Fanoshells: Nanoparticles with built-in fano resonances. *Nano Lett.* **2010**, *10*, 2694–2701. [[CrossRef](#)] [[PubMed](#)]
11. Ozbay, E.; Bayindir, M.; Bulu, I.; Cubukcu, E. Investigation of localized Coupled-Cavity modes in Two-Dimensional photonic bandgap structures. *IEEE J. Quantum Elect.* **2002**, *38*, 837–843. [[CrossRef](#)]
12. Wang, Q.; Zhao, H.; Du, X.; Zhang, W.; Qiu, M.; Li, Q. Hybrid photonic-plasmonic molecule based on metal/Si disks. *Opt. Express* **2013**, *21*, 11037–11047. [[CrossRef](#)] [[PubMed](#)]
13. Ryu, J.; Lee, S.; Kim, S.W. Coupled nonidentical microdisks: Avoided crossing of energy levels and unidirectional far-field emission. *Phys. Rev. A* **2009**, *79*, 53858. [[CrossRef](#)]
14. Boriskina, S.V. Coupling of whispering-gallery modes in size-mismatched microdisk photonic molecules. *Opt. Lett.* **2007**, *32*, 1557–1559. [[CrossRef](#)] [[PubMed](#)]
15. Chen, P.; Alu, A. Atomically thin surface cloak using graphene monolayers. *ACS Nano* **2011**, *5*, 5855–5863. [[CrossRef](#)] [[PubMed](#)]
16. Huang, Y.X.; Zhao, J.; Qiu, W.B.; Lin, S.X.; Chen, H.B.; Wang, J.X.; Kan, Q.; Pan, J.Q. Investigation of the tunable plasmonic whispering gallery mode properties for graphene monolayer nanodisk cavities. *Optik* **2016**, *127*, 5591–5596. [[CrossRef](#)]
17. Zhao, J.; Qiu, W.B.; Huang, Y.X.; Wang, J.X.; Kan, Q.; Pan, J.Q. Investigation of plasmonic whispering-gallery mode characteristics for graphene. *Opt. Lett.* **2014**, *39*, 5527–5530. [[CrossRef](#)] [[PubMed](#)]
18. Zhu, X.L.; Wang, W.L.; Yan, W.; Larsen, M.B.; Boggild, P.; Pedersen, T.G.; Xiao, S.S.; Zi, J.; Mortensen, A. Plasmon-phonon coupling in large-area graphene dot and antidot arrays fabricated by nanosphere lithography. *Nano Lett.* **2014**, *14*, 2907–2913. [[CrossRef](#)] [[PubMed](#)]
19. Maes, B.; Rosolen, G. Asymmetric and connected graphene dimers for a tunable plasmonic response. *Phys. Rev. B* **2015**, *92*, 205405.
20. Hadad, Y.; Steinberg, B.Z. Quasistatic resonance of a chemical potential interruption in a graphene layer and its polarizability: The mixed-polarity semilocalized plasmon. *Phys. Rev. B* **2013**, *88*, 075439. [[CrossRef](#)]
21. Hadad, Y.; Davoyan, A.R.; Engheta, N.; Steinberg, B.Z. Extreme and Quantized Magneto-optics with Graphene Meta-atoms and Metasurfaces. *ACS Photonics* **2014**, *1*, 1068–1073. [[CrossRef](#)]
22. Qiu, W.B.; Huang, Y.X.; Chen, H.B.; Qiu, P.P.; Tang, Y.X.; Wang, J.X.; Kan, Q.; Pan, J.Q. Coupling of Whispering-Gallery modes in the graphene nanodisk plasmonic dimers. *Plasmonics* **2016**, *12*, 1–7. [[CrossRef](#)]
23. Huang, F.; Baumberg, J.J. Actively tuned plasmons on elastomerically driven Au nanoparticle dimers. *Nano Lett.* **2010**, *10*, 1787–1792. [[CrossRef](#)] [[PubMed](#)]
24. Acimovic, S.S.; Kreuzer, M.P.; Gonzalez, M.U.; Quidant, R. Plasmon near-field coupling in metal dimers as a step toward single-molecule sensing. *ACS Nano* **2009**, *3*, 1231–1237. [[CrossRef](#)] [[PubMed](#)]
25. Large, N.; Abb, M.; Aizpurua, J.; Muskens, O.L. Photoconductively loaded plasmonic nanoantenna as building block for ultracompact optical switches. *Nano Lett.* **2010**, *10*, 1741–1746. [[CrossRef](#)] [[PubMed](#)]
26. Huang, Y.X.; Qiu, W.B.; Lin, S.X.; Chen, H.B.; Wang, J.X.; Kan, Q.; Pan, J.Q. Analysis of mode characteristics and output efficiency of graphene equilateral triangle nanocavity with vertex output waveguide. *Opt. Quantum Electron.* **2016**, *48*, 1–10. [[CrossRef](#)]
27. Hanson, G.W. Dyadic Green's functions and guided surface waves for a surface conductivity model of graphene. *J. Appl. Phys.* **2008**, *103*, 64302. [[CrossRef](#)]
28. Qiu, W.B.; Liu, X.H.; Zhao, J.; He, S.H.; Ma, Y.H.; Wang, J.X.; Pan, J.Q. Nanofocusing of mid-infrared electromagnetic waves on graphene monolayer. *Appl. Phys. Lett.* **2014**, *104*, 41109. [[CrossRef](#)]

29. Zhao, J.; Liu, X.H.; Qiu, W.B.; Ma, Y.H.; Huang, Y.X.; Wang, J.X.; Qiang, K.; Pan, J.Q. Surface-plasmon-polariton whispering-gallery mode analysis of the graphene monolayer coated InGaAs nanowire cavity. *Opt. Express* **2014**, *22*, 5754–5761. [[CrossRef](#)] [[PubMed](#)]
30. Vakil, A.; Engheta, N. Transformation optics using graphene. *Science* **2011**, *332*, 1291–1294. [[CrossRef](#)] [[PubMed](#)]
31. Efetov, D.K.; Kim, P. Controlling Electron-Phonon interactions in graphene at ultrahigh carrier densities. *Phys. Rev. Lett.* **2010**, *105*, 256805. [[CrossRef](#)] [[PubMed](#)]
32. Low, T.; Avouris, P. Graphene plasmonics for terahertz to Mid-Infrared applications. *ACS Nano* **2014**, *8*, 1086–1101. [[CrossRef](#)] [[PubMed](#)]
33. Huang, Y.X.; Qiu, W.B.; Lin, S.X.; Zhao, J.; Chen, H.B.; Wang, J.X.; Kan, Q.; Pan, J.Q. Investigation of plasmonic whispering gallery modes of graphene equilateral triangle nanocavities. *Sci. China Inf. Sci.* **2016**, *59*, 1–9. [[CrossRef](#)]
34. Kwon, S.H. Deep subwavelength plasmonic whispering-gallery-mode cavity. *Opt Express* **2012**, *20*, 24918–24924. [[CrossRef](#)] [[PubMed](#)]
35. Zhang, S.; Li, G.C.; Chen, Y.Q.; Zhu, X.P.; Liu, S.D.; Lei, D.Y.; Duan, H.G. Pronounced fano resonance in single gold split nanodisks with 15 nm split gaps for intensive second harmonic generation. *ACS Nano* **2016**, *10*, 11105–11114. [[CrossRef](#)] [[PubMed](#)]
36. Rahmani, M.; Lei, D.Y.; Giannini, V.; Lukiyanchuk, B.; Ranjbar, M.; Liew, T.Y.F.; Hong, M.H.; Maier, S.A. Subgroup decomposition of plasmonic resonances in hybrid oligomers: Modeling the resonance lineshape. *Nano Lett.* **2012**, *12*, 2101–2106. [[CrossRef](#)] [[PubMed](#)]
37. Liu, S.D.; Leong, E.S.P.; Li, G.C.; Deng, J.; Teng, J.H.; Ong, H.C.; Lei, D.Y. Polarization-independent multiple fano resonances in plasmonic nonamers for multimode-matching enhanced multiband second-harmonic generation. *ACS Nano* **2016**, *10*, 1442–1453. [[CrossRef](#)] [[PubMed](#)]
38. Lei, D.Y.; Fernandez-Dominguez, A.I.; Sonnefraud, Y.; Appavoo, K.; Haglundjr, R.F.; Pendry, J.B.; Maier, S.A. Revealing plasmonic gap modes in particle-on-film systems using dark-field spectroscopy. *ACS Nano* **2012**, *6*, 1380–1386. [[CrossRef](#)] [[PubMed](#)]
39. Li, G.C.; Zhang, Y.L.; Lei, D.Y. Hybrid plasmonic gap modes in metal film-coupled dimers and their physical origins revealed by polarization resolved dark field spectroscopy. *Nanoscale* **2016**, *8*, 7119–7126. [[CrossRef](#)] [[PubMed](#)]
40. Li, G.C.; Zhang, Y.L.; Jiang, J.; Luo, Y.; Lei, D.Y. Metal-substrate-mediated plasmon hybridization in a nanoparticle dimer for photoluminescence line-width shrinking and intensity enhancement. *ACS Nano* **2017**. [[CrossRef](#)] [[PubMed](#)]



© 2017 by the authors. Licensee MDPI, Basel, Switzerland. This article is an open access article distributed under the terms and conditions of the Creative Commons Attribution (CC BY) license (<http://creativecommons.org/licenses/by/4.0/>).